Theoretical Photoelastic Stresses in Three Dimensional Body with Elastic Contact

Ouk Sub Lee* and Kee Yong Nam**

(*Received June 12, 1998*)

An understanding of the Hertz contact theory is important for investigating the failure strength and behavior of rolling and/or slipping mechanical-structural components. Two simple special cases including a circular contact and line contact patch have been solved in the closed form solution. However, there are many unsolved complicated cases where the contact areas become elliptical contact patches. In this paper, a simple stress field generated in contact bodies under general loading conditions is derived. The stress field derived in this paper is utilized to generate theoretical three dimensional photoelastic isochromatic fringe patterns. Some of the theoretical isochromatic fringe patterns are compared with published experimental results. The agreement between the theoretical and the experimental results are found to be good.

Key Words: Contact Stress, Elliptical Integral, General Loading Conditions, Hertz Contact, Photoelasticity, Rolling and/or Slipping.

1. Introduction

The barge system usually consists of a vessel carrying a barge and a pusher which transmits the necessary power for the movement of the barge-carrying vessel. The contact of connecting parts between the vessel and the pusher plays an important role in transmitting the power. The contact is under very complicated loading conditions including rolling and sliding motions. It is necessary to investigate the effect of these contact pressure on the strength, damage and fracture analyses of the barge system by extending the well-known Hertz contact theory (Love 1965, Timoshenko & Goodier 1970).

An in-depth understanding of the Hertz theory describing the distribution of contact pressure in the body is important to investigate the strength and behavior of rolling and/or slipping components. The Hertz theory is generally applicable to the contact problem where two linear elastic bodies are in contact with each other. This theory is limited to the case where curvatures of the point of contact are provided by parabolic surface and the dimensions of the contact patch must remain small compared with the radii of curvature of the bodies.

There are two special cases in the Hertz contact. One is a circular contact patch (Hüber 1904), and the other is a line contact (Poritsky 1950).

There are, however, many cases where an elliptical contact patch occurs (Sackfield & Hills 1983), such as in a ball rolling in a non-conforming groove, a railway wheel moving along a convex-headed rail, a cross-cylinder wear tester where the cylinders are of different diameters and the barge connecting system.

In this paper, the elliptical contact patch is considered and the stress field around the contact patch for general loading condition is derived. We attempt to develop the general stress field in the simplest form for experimental applications without many implicit factors. Furthermore, the theoretically developed general stress field for the case of elliptical Hertz contact is used to generate two dimensional photoelastic isochromatic fringe patterns. Some published experimental results

* School of Mechanical, Aerospace and Automation, Inha University 402-751, Inchon Korea
** Graduate Student Inha University 402-751, Inchon Korea

(Burguete & Patterson 1997) are compared with those generated in this paper.

2. General Theory

2.1 Hertz contact problem with normal load

2.1.1 General theory

All coordinate systems used in this study are normalized with respect to the contact dimension a_0 in Fig. 1.

The first task in solving the probllm is to find the principal axes lying in the plane of contact. The expression for the relative separation of points is

$$h(x, y)=\frac{1}{2}Ax^2+\frac{1}{2}By^2$$

where A and B are the principal relative curvatures.

By analogy with the plane and axi-symmetric cases, we expect the pressure distribution to be in the form of an ellipsoid,

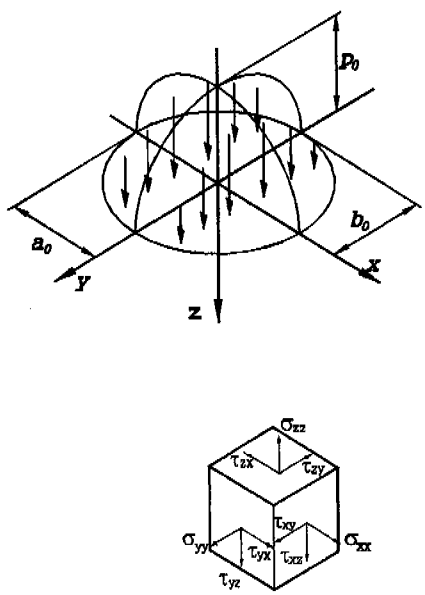

Fig. 1 Elliptical contact patch with the normal pressure distribution over the contact area and an element with stress components. (x, y, z=coordinate systems, p_0=maximum contact pressure, a_0, b_0=length of semi-axes of the contact patch).

$$p(x, y)=-p_0\sqrt{1-(x^2/a_0^2)-(y^2/b_0^2)}$$

over the contact ellipse

$$(x^2/a_0^2)+(y^2/b_0^2)\leq 1$$

The solution for the stress, strain and displacement fields induced in a half-space by the contact pressure using the potential methods of Boussinesq and Cerutti, is fully described (Love 1952). The method to produce a satisfactory solution for the general Hertzian contact problem is to start with a pressrue distribution and the surface displacements. In this case it is observed that ϕ has all the properties associated with the Newtonian potential of a solid homogeneous ellipsoid.

$$\phi=\frac{3P}{4}\int_r^\infty\left(1-\frac{x^2}{a_0^2+\phi}-\frac{y^2}{b_0^2+\phi}-\frac{z^2}{\phi}\right)\times\frac{d\psi}{\sqrt{\psi(a_0^2+\psi)(b_0^2+\psi)}}$$

where ψ is the displacement and r is the largest root of $1-\frac{x^2}{a_0^2+r}-\frac{y^2}{b_0^2+r}-\frac{z^2}{r}=0$.

The three simple stress components for an element in the body (refer Fig. 1) are given by

$$\frac{\tau_{xz}}{p_0}=\frac{\sigma_{13}}{p_0}=-\frac{kxzL}{(1+s^2)} \tag{1}$$

$$\frac{\tau_{yz}}{p_0}=\frac{\sigma_{23}}{p_0}=-\frac{kxzL}{(k^2+s^2)} \tag{2}$$

$$\frac{\sigma_{zz}}{p_0}=\frac{\sigma_{33}}{p_0}=-\frac{kz^2L}{s^2} \tag{3}$$

where, p_0 is the maximum contact pressure, $k=b_0/a_0$, $s^2=r/a_0^2$

$$L=z/[s^3H\sqrt{\{(1+s^2)(k^2+s^2)\}}] \text{ and}$$

$$H=\left(\frac{x}{1+s^2}\right)^2+\left(\frac{y}{k^2+s^2}\right)^2+\left(\frac{z}{s^2}\right)^2$$

The other three stress components are represented as

$$\frac{\sigma_{xx}}{p_0}=\frac{\sigma_{11}}{p_0}=\left(\frac{\nu}{\pi}\right)\frac{\pi_3}{p_3}-\frac{(1-2\nu)}{2\pi}\frac{x_{11}}{p_0}-\frac{1}{2\pi}\left(\frac{z\phi_{11}}{p_0}\right) \tag{4}$$

$$\frac{\sigma_{yy}}{p_0}=\frac{\sigma_{22}}{p_0}=\left(\frac{\nu}{\pi}\right)\frac{\phi_3}{p_3}-\frac{(1-2\nu)}{2\pi}\frac{x_{22}}{p_0}-\frac{1}{2\pi}\left(\frac{z\phi_{22}}{p_0}\right) \tag{5}$$

$$\frac{\tau_{xy}}{p_0}=\frac{\sigma_{12}}{p_0}=-\frac{(1-2\nu)}{2\pi}\frac{x_{12}}{p_0}-\frac{1}{2\pi}\left(\frac{z\phi_{12}}{p_0}\right) \tag{6}$$

where, ν is the Poisson's ratio,

$$\left(\frac{z\phi_{11}}{p_0}\right)=-2\pi k\left\{zI_1-\left(\frac{xs}{1+s^2}\right)^2 L\right\},$$

$$\left(\frac{z\phi_{22}}{p_0}\right)=-2\pi k\left\{zI_2-\left(\frac{ys}{k^2+s^2}\right)^2 L\right\},$$

$$\left(\frac{z\phi_{12}}{p_0}\right)=\frac{2\pi kxyLs^2}{(1+s^2)(k^2+s^2)},\ \left(\frac{\phi_3}{p_0}\right)=-2\pi kzI_3$$

$$\frac{\chi_{11}}{p_0}=-2\pi k\left[zI_1-\frac{1}{n^3}\left\{y\theta_1+x\theta_2+n-\frac{zn}{s}\times\sqrt{\left(\frac{s^2+k^2}{s^2+1}\right)}\right\}\right]$$

$$\frac{\chi_{22}}{p_0}=-2\pi k\left[zI_2-\frac{1}{n^3}\left\{y\theta_1+x\theta_2+n-\frac{zn}{s}\times\sqrt{\left(\frac{s^2+1}{s^2+1k}\right)}\right\}\right]$$

$$\frac{\chi_{12}}{p_0}=\frac{2\pi k}{n^3}\{x\theta_1-y\theta_2\}$$

and

$$\theta_1=\tan^{-1}\left\{\frac{Y(a-1)}{1+Y^2a}\right\},$$

$$\theta_2=\tanh^{-1}\left\{\frac{X(a-1)}{1-X^2a}\right\}$$

$$X=\frac{xn}{1-p^2},\ Y=\frac{yn}{k^2-p^2}$$

p is the smallest rooot of $\frac{x^2}{(1-p^2)}+\frac{y^2}{(k^2-p^2)}=1$.

$$a^2=\frac{(s^2+p^2)(k^2-p^2)}{(k^2-p^2)(s^2+k^2)+n^2y^2},\ n^2=1-k^2$$

And, I_i is the three type of elliptic integral given by

$$I_1=\int_s^\infty \frac{dw}{(1+w^2)^{3/2}(k^2+w^2)^{1/2}}$$

$$I_2=\int_s^\infty \frac{dw}{(1+w^2)^{1/2}(k^2+w^2)^{3/2}}$$

$$I_3=\int_s^\infty \frac{dw}{w^2(1+w^2)^{1/2}(k^2+w^2)^{1/2}}$$

2.1.2 A special case

It was considered valuable to assess the stress field for a special case such as for a vertical plane of symmetry, $y=0$ since we can compared the results with those of two dimensional photoelastic experimental isochromatic fringes. The results would be utilized to locate the high tensile stress region which should be flaw-free zone to prevent dangerous crack propagation.

From symmetry $y=0$, it is clear that

$$\tau_{xy}=\tau_{yz}=0 \tag{7}$$

The other direct stresses may be simplified as the following

$$\frac{\tau_{xz}}{p_0}=-\frac{kxzL}{(1+s^2)} \tag{8}$$

$$\frac{\sigma_{xx}}{p_0}=-2k(1+\nu)zI_3-\frac{\sigma_{yy}}{p_0}-\frac{\sigma_{zz}}{p_0} \tag{9}$$

$$\frac{\sigma_{yy}}{p_0}=k\{-2\nu zI_3+2(1-\nu)zI_2-(1-2\nu)I_4\} \tag{10}$$

$$\frac{\sigma_{zz}}{p_0}=-\frac{kz^2L}{s^2} \tag{11}$$

where I_4 is an elementary integral given by when $q\neq 0$,

$$I_4=\frac{q_1}{(1-k^2)^{3/2}}\left[\sqrt{(x/q_1)^2+r^2}sign(q^2)-|x/q_1|\cdot\log_e\left|\frac{|x/q_1|+\sqrt{(x/q_1)^2+r^2}sign(q^2)}{r}\right|\right]_1^r$$

when $q=0$, $I_4=\frac{x}{(1-k^2)^{3/2}}\log_e(r)$

when, $k<1$, $q^2=1-k^2-x^2$, $r^2=\frac{1+s^2}{k^2+s^2}$,

$q_1=\sqrt{q^2}$

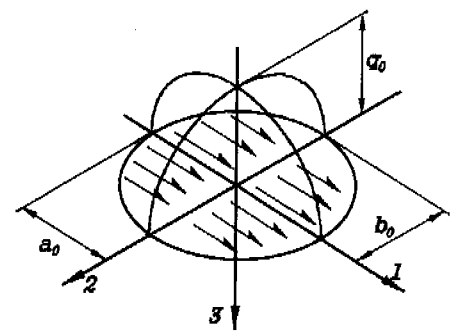

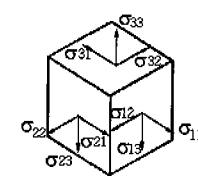

Fig. 2 Elliptical contact patch with the tangential pressure distribution over the contact area and an element with stress components. (1, 2, 3=coordinate systems, q_0=maximum contact pressure, a_0, b_0=length of semi-axes of the contact patch).

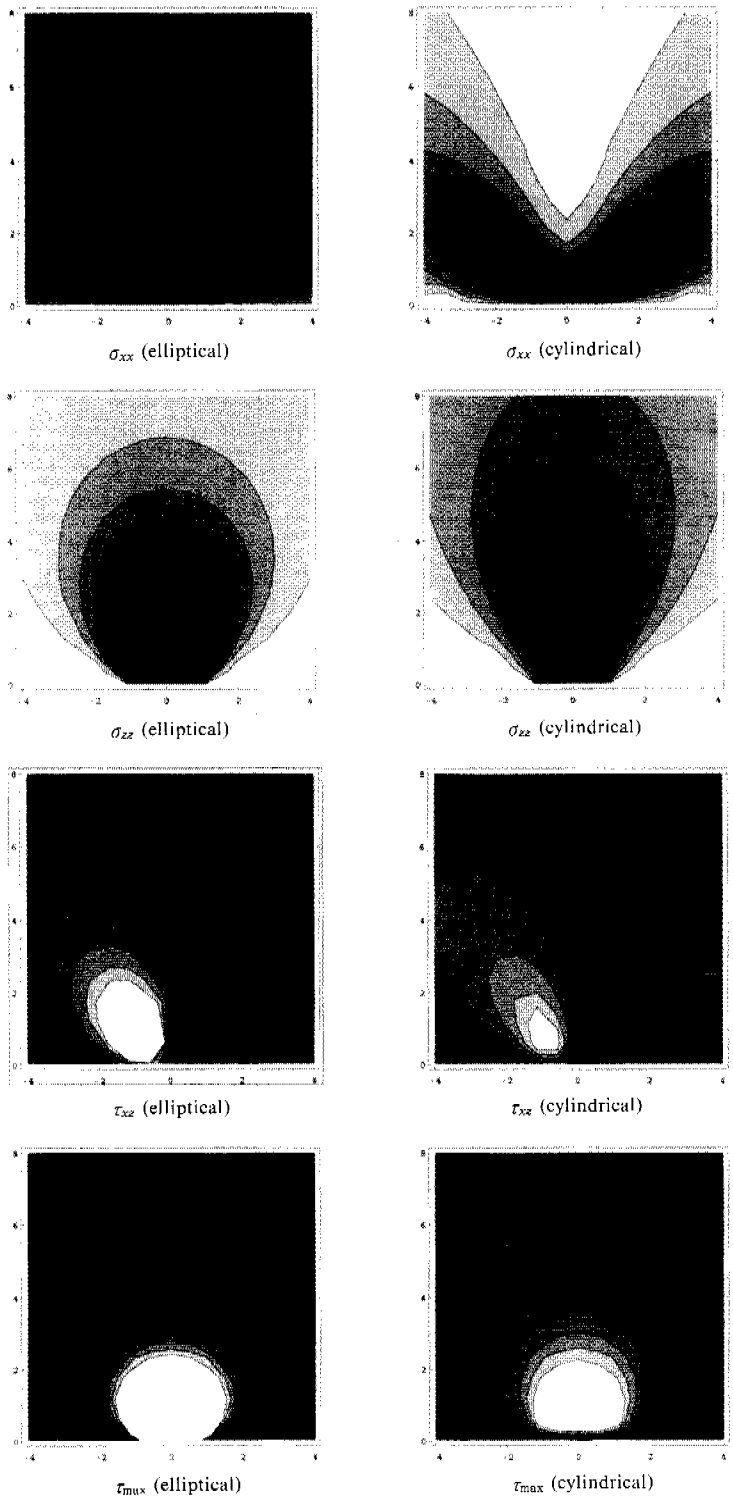

Fig. 3 Isostatic-stress and max. tangential stress contours in elliptical and cylindrical contact patches under the normal loading condition (p_0). To keep the same geometric condition, the lengths of semi-axes are taken as $a_0=1.001$, and $b_0=1$.

2.2 Hertz contact problem with tangential load

2.2.1 General theory

The stress components can be obtained as follows using the same procedure for the normal loading condition.

$$\frac{\sigma_{11}}{kq_0}=-\frac{2x}{n^2}\{(n^2+\nu)I_1-\nu k^2 I_2\} -(1-2\nu)z\times\partial J/\partial y +\frac{x}{HG^3}\left\{\frac{z^2(s^2+k^2)}{s}+\frac{2\nu y^2 s}{k^2+s^2}\right\} \quad (12)$$

$$\frac{\sigma_{22}}{kq_0}=2\nu x\left\{\frac{k^2}{n^2}(I_1-I_2)-\frac{y^2 s}{HG^3(k^2+s^2)}\right\} +(1-2\nu)z\partial J/\partial y \quad (13)$$

$$\frac{\sigma_{33}}{kq_0}=-\frac{xz^2}{s^3(s^2+1)HG} \quad (14)$$

$$\frac{\sigma_{12}}{kq_0}=\frac{y}{n^2}\{2\nu(I_1-k^2I_2)-n^2I_2\} -\frac{2\nu x^2 ys}{HG^3(s^2+1)}+(1-2\nu)z\partial J/\partial y \quad (15)$$

$$\frac{\sigma_{13}}{kq_0}=-\frac{x^2z}{HGs(s^2+1)^2}+z(I_1-I_3) \quad (16)$$

$$\frac{\sigma_{23}}{kq_0}=-\frac{xyz}{sHG^3} \quad (17)$$

where, $G=\{(s^2+1)(s^2+k^2)\}^{1/2}$

$$n^3J=y\times\arctan h\left\{\frac{X(\alpha-1)}{1-X^2\alpha}\right\}-x \times\arctan h\left\{\frac{Y(\alpha-1)}{1-Y^2\alpha}\right\}$$

All the unknown parameters in the above equa-

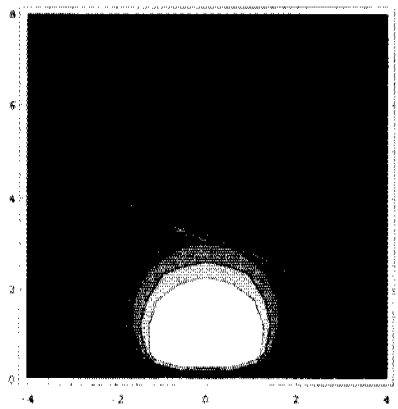

(a) Theoretical

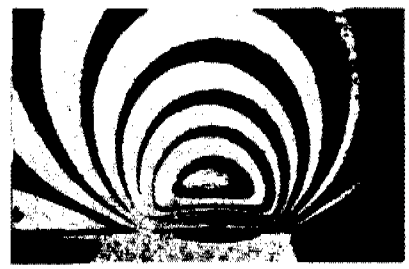

(b) Experimental (Lee 1991)

Fig. 4 Theoretical and experimental isochromatic fringes in two dimensional approach.

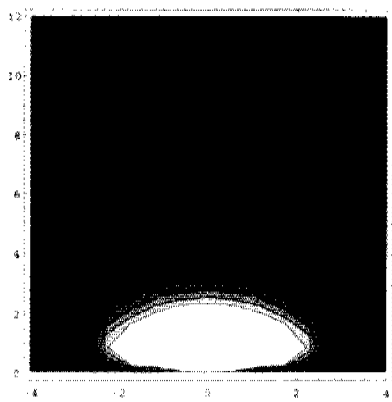

(a) $a_0=2$, $b_0=1$

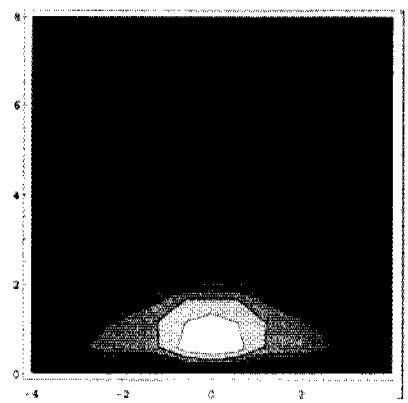

(b) $a_0=3$, $b_0=1$

Fig. 5 Theoretical isochromatic fringes for various elliptical contact areas at the normal loading condition.

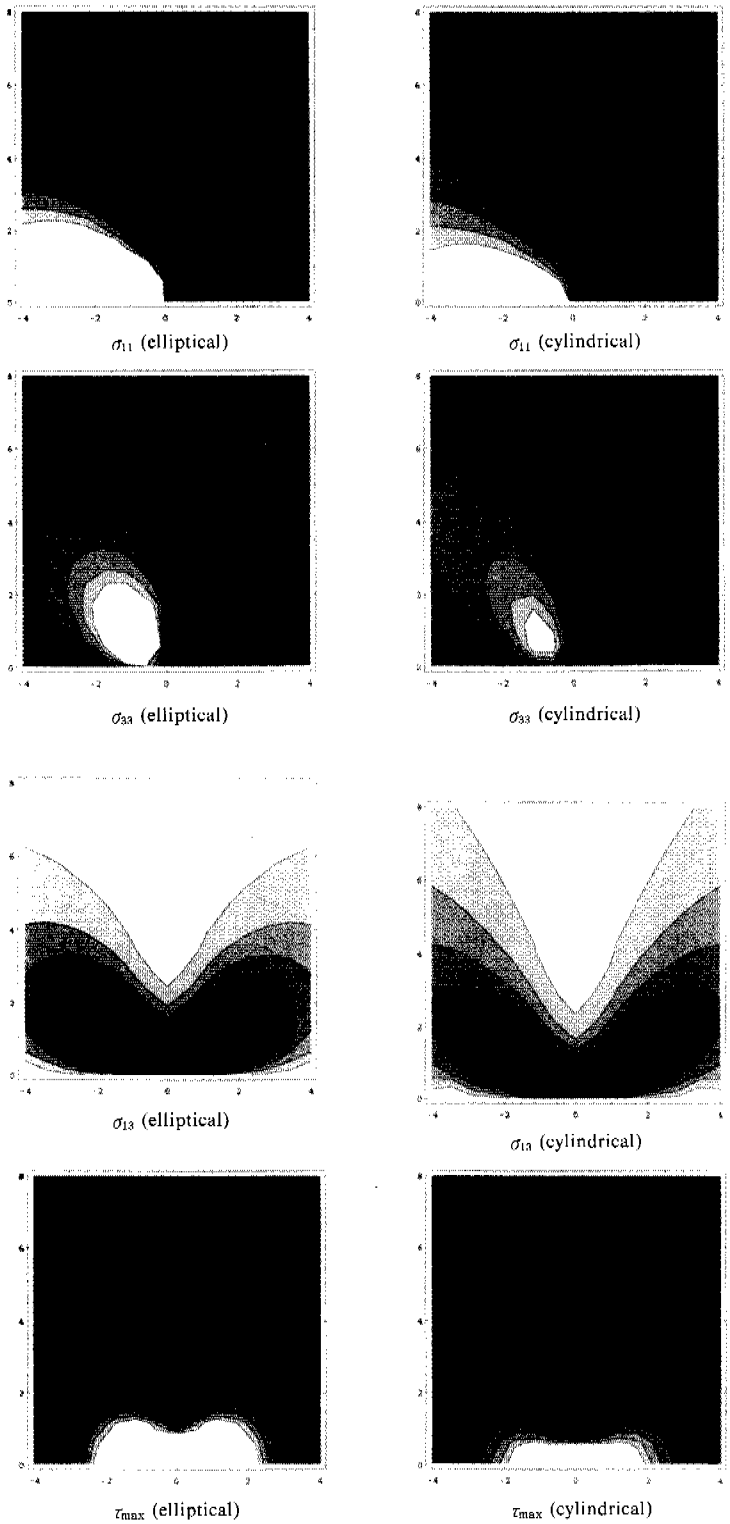

Fig. 6 Isostatic-stress contours in an elliptical contact and a cylindrical contact patches under normal loading condition ($q_0=1$).

tions in this section are the same as those for the normal load condition.

2.2.2 A special case

Since we are interested in generating the theoretical isochromatic fringes under tangential loading condition, the stress field for a special case of the vertical plane of symmetry, $y=0$ is considered.

Only three stress components are needed to evaluate the maximum shear stress in the vertical plane of symmetry. The maximum shear stresses are used to generate isochromatic fringes. Three stress components (σ_{11}, σ_{33}, σ_{13}) obtained by substituting $y=0$ into the general stress equations are

$$\frac{\sigma_{11}}{kq_0}=-\frac{2x}{n^2}\{(n^2+\nu)I_1\nu k^2 I_2\}+\frac{x}{HG}\left\{\frac{z^2(s^2+k^2)}{s^2}+\frac{2\nu y^2 s}{k^2+s^2}\right\} \quad (18)$$

$$\frac{\sigma_{13}}{kq_0}=-\frac{x^2 z}{HGs(s^2+1)^2}+z(I_1-I_3) \quad (19)$$

$$\frac{\sigma_{33}}{kq_0}=-\frac{xz^2}{s^3(s^2+1)\overline{HG}} \quad (20)$$

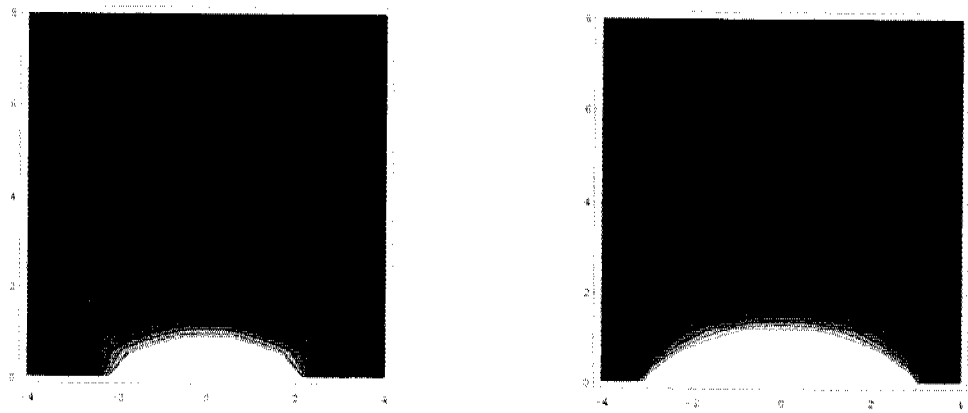

(a) $a_0=2$, $b_0=1$ (b) $a_0=3$, $b_0=1$

Fig. 7 Theoretical isochromatic fringes for various elliptical contact areas under tangential loading condiion ($q_0=1$).

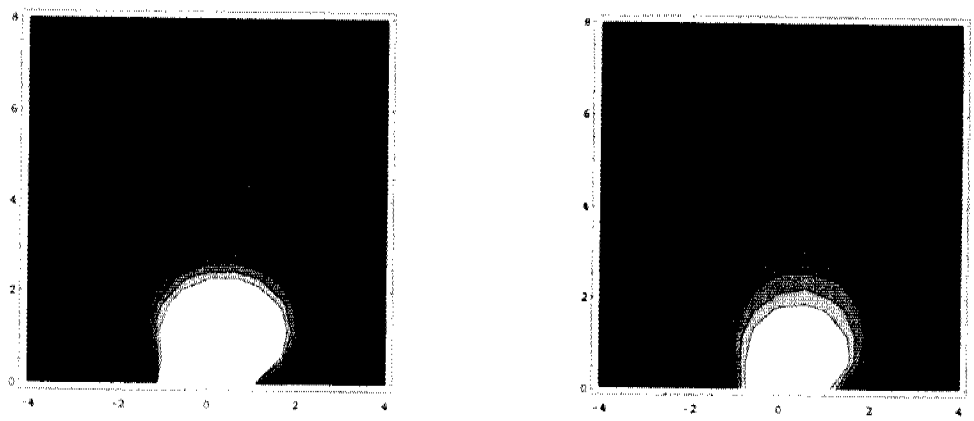

(a) (elliptical) (b) (cylindrical)

Fig. 8 Theoretical isochromatic fringes for an elliptical contact patch and a cylindrical contact patch under various mixed loading condition. (friction factor=0.3 $p_0=1$, $q_0=1.001$, $b_0=1$).

3. Theoretical Stress Field and Comparison with Those of Two Dimensional Photoelastic Experiment

Maximum shear stress (τ_m) and photoelastic isochromatic fringe relates as

$$\tau_m=\frac{Nf_0}{2t} \tag{21}$$

where, f_σ : photoelastic material property,
t : material thickness,
N : number of isochromatic fringe order.

3.1 Theoretical photoelastic stress analysis for normal load

Using the Mohr's circle theory, maximum shear stresses on xz plane can be determined as Eq. (22) by using the stress components in section 2. 1.2,

$$\tau_m=\sqrt{\left(\frac{\sigma_{xx}-\sigma_{zz}}{2}\right)^2+\tau_{xz}^2} \tag{22}$$

Figure 3 shows the theoretically generated isostatic-stress contours and isochromatic fringe patterns for two different contact systems. It is noted that the elliptical contact is three dimensional contact, while cylindrical contact is two dimensional contact. In the elliptical contact, the length of semi-axes is taken as $a_0=1.001$, $b_0=1$. If the

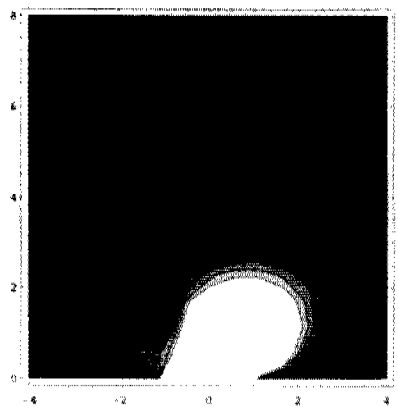

(a) $p_0=1$, $q_0=1$

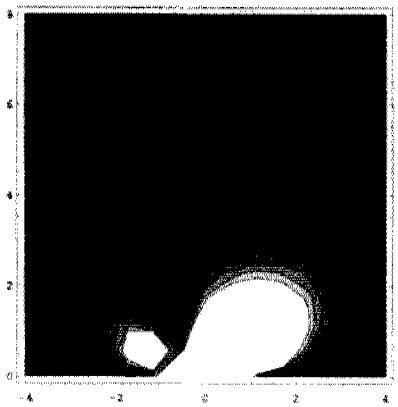

(b) $p_0=1$, $q_0=2$

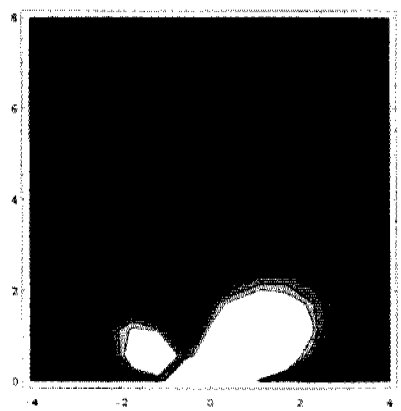

(c) $p_0=1$, $q_0=3$

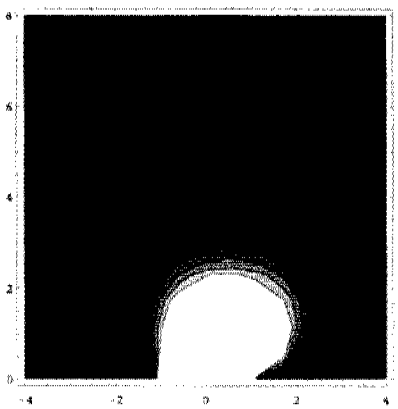

(d) $p_0=2$, $q_0=1$

Fig. 9 Theoretical isochromatic fringes for various elliptical contact patch and a cylindrical contact patch under various mixed loading condition ϕ. ($a_0=1.001$, $b_0=1$).

lengths of semi-axes are the same (e.g. $a_0=1$ and $b_0=1$) the solution would be meaningless since it is impossible to evaluate the elliptical integral. In the normal stress fringe patterns, the bright area reveals the tensile stress region, while the dark area is the compressive stress region.

It is found that fringe patterns under two different contact conditions such as elliptical and cylindrical look similar under the vertical loading condition. However, the stress level of the elliptical contact is found to be larger than that of the cylindrical contact at the same local area. It is, thus, found that the cylindrical simulation for the three dimensional contact problem may cause some errors in the estimation of real stress distribution.

The theoretical and experimental fringes in two dimensional are shown in Fig. 4. The agreements between two isochromatic fringes are good.

Fig. 5 shows the variation of theoretical isochromatic fringe patterns according to the changes of the elliptical contact areas under the normal loading conditions. The higher the elliptical axis ratios are, the flatter are the shape of the isochromatic fringe loops.

3.2 Theoretical photoelastic stress analysis for tangential load

Using the Mohr's circle theory, maximum shear stresses on 1-3 plane are given as Eq. (23) by using the stress components in section 2.2.2,

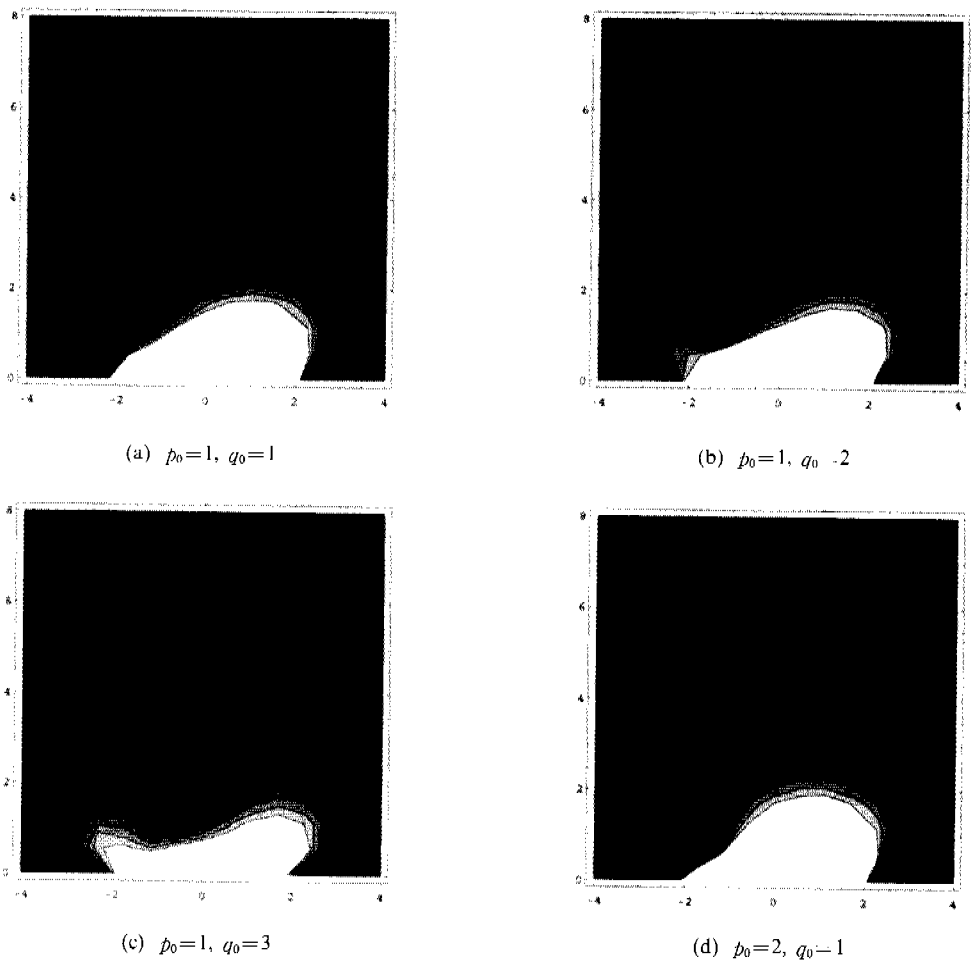

(a) $p_0=1$, $q_0=1$ (b) $p_0=1$, q_0 -2

(c) $p_0=1$, $q_0=3$ (d) $p_0=2$, $q_0=1$

Fig. 10 Theoretical isochromatic fringes for various elliptical contact areas under various loading condition. ($a_0=1$, $b_0=1$).

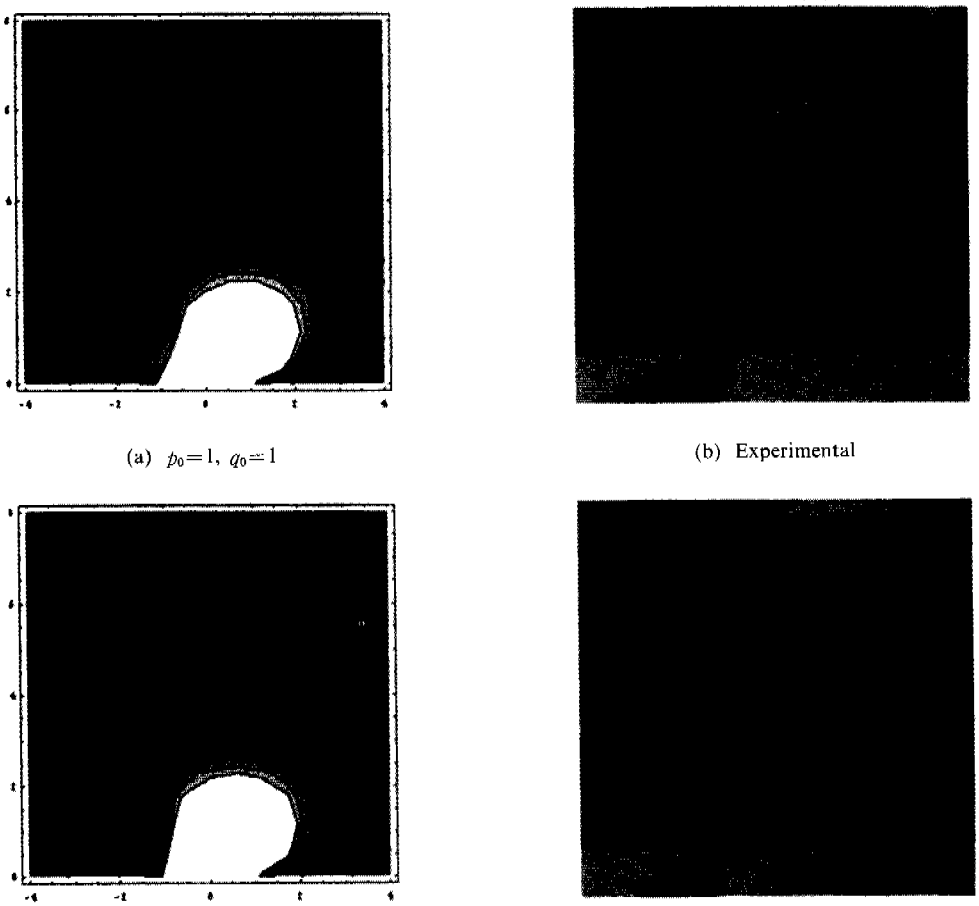

(a) $p_0=1$, $q_0=1$ (b) Experimental

(c) $p_0=1.66$, $q_0=1$ (d) Experimental

Fig. 11 Experimental and theoretical isochromatic fringe patterns under various loading.(Lee 1991).

$$\tau_m=\sqrt{\left(\frac{\sigma_{11}-\sigma_{33}}{2}\right)^2+\sigma_{13}^2} \tag{23}$$

The stresses and maximum tangential stresses obtained by the theoretical approach are shown in Figs. 6, and 7, respectively. In the elliptical contact, the lengths of semi-axes are taken as $a_0=1.001$ and $b_0=1$ as for the normal loading case. In Fig. 6, the stress level of the elliptical contact is found to be larger than that of the cylindrical contact at the same local area.

The theoretical isochromatic fringes are formed as shown in Fig. 7 when the elliptical contact areas under the tangential loading condition is changed. The higher the ratios of the elliptical axis are, the sharper becomes the shape of the isochromatic fringes. The effect of the ratios of elliptical axis on the fracture behavior may be investigated by using the presently developed stress field equations.

3.3 Theoretical photoelastic stress analysis for mixed load

The maximum shear stress on xz plane under mixed loading conditions is derived as Eq. (24) by superimposing the stress components in section 2.1.2 and in section 2.2.2,

$$\tau_m=\sqrt{\left(\frac{(\sigma_{xx}+\sigma_{11})-(\sigma_{zz}+\sigma_{33})}{2}\right)^2+(\tau_{xz}+\sigma_{13})^2} \tag{24}$$

The typical theoretical isochromatic fringe loops for the elliptical and cylindrical contacts under the mixed load condition with a friction

factor of 0. 3 are shown in Fig. 8. It is found that two fringe patterns with different contacts look similar under the same loading condition. The stress level of the elliptical contact is greater than that of the cylindrical contact with the same geometric area.

The theoretical isochromatic fringes corresponding to various elliptical contact pressure at the mixed loading condition are generated as shown in Fig. 9. The effect of tangential loading pressure on the theoretically generated isochromatic fringe loops is clearly seen in Fig. 9. When the normal loading pressure increases, the generated isochromatic fringe loops become closer to one obtained under the pure normal loading condition.

The isochromatic loops shown in Fig. 10 are generated with the elliptical contact area of $a_0=2$, $b_0=1$ with a loading condition which is the same as in Fig. 9. The high maximum shear stress zone becomes wider than that of Fig. 9.

A comparison between theoretical isochromatics and two dimensional photoelastic experiments is made as shown in Fig. 11. The experimental isochromatic fringe loops obtained under punch presses with 44 degree angle from the vertical axis and with 31 degree angle from the vertical axis are shown in Fig. 11 (b), and Fig. 11 (d), respectively. The agreement between the two cases is good.

4. Conclusion

In this paper, the three dimensional contact stress fields for various contact patches areas based on the Hertz contact theory are formulated. The theoretical stress fields are compared with the published experimental stress fields. The results obtained from this study are as follows:

1) Three dimensional contact stress fields are derived, and the stresses on the middle contact plane is determined to generate the theoretical photoelastic isochromatic fringes.

2) Theoretical isochromatic fringe loops are generated under different loading conditions by using the three dimensional contact stress fields. Also the effect of the contact stress distribution is monitored with respect to changed elliptical area in the body.

3) It is found that isochromatic fringe loops generated by using the three dimensional stress analysis differ slightly from those obtained by the two dimensional photoelastic experimental stress analysis.

Acknowledgment

This work was supported by '95 Special Fund for University Research Institute, Korea Research Foundation.

References

Burguete, R. L. and Patterson E. A. , 1997, "A Photoelastic Study of Contact Between a Cylinder and a Half space," Experimental Mechanics, Vol. 37, No. 3, pp. 314~323. H ber, M. T., 1904, "Zur Theorie der Ber hrung Fester Elasticher Körper," *Ann al. Physik,* Vol. 14, pp. 153~163.

Lee, H. S., 1991, "Analysis for Subsurface Crack by Photoelasticity," Ph. D., dissertation, Inha University.

Love, A. E. H., 1952, "The Mathematical Theory of Elasticity, 4th Edition" (Cambridge university)

Poritsky, H., 1950, "Stress and Deflections of Cylindrical Bodies in Contact with Application to Contact of Gears and of Locomotive Wheels," *J. Applied Mech.,* Vol. 72, pp. 191~201.

Sackfield, A. and Hills, D. A., 1983, "Some Useful Results in the Classical Hertz Contact Problem," *J. of Strain Analysis,* Vol. 18, No. 2, pp. 101~105.

Sackfield, A. and Hills, D. A., 1983, "Some Useful Results in the Tangentially Loaded Hertzian Contact Problem," *J. of Strain Analysis,* Vol. 18, No. 2, pp. 107~110.

Smith, J. O. and Liu, C. K., 1953, "Stresses Due to Tangential and Normal Loads on an Elastic Solid with Application to Some Contact Stress Problems," *Trans. ASME, Journal of Applied Mech.,* Vol. 75, pp. 157~166.

Timoshenko S. P. and Goodier J. N., 1970, *Theory of Elasticity,* 3rd edition, pp. 414~420.